Published by Avanti Publishers

Journal of Advanced Thermal Science Research

ISSN (online): 2409-5826

Thermal Diffusivity of $Ti_3C_2T_x$@C Nanocoils

Yeti Li, Fengming Wu, Siqi Zhao and Chenghao Deng*

Center on Nanoenergy Research, School of Physical Science and Technology, Guangxi University, Naning 530004, P.R. China

ARTICLE INFO

Article Type: Research Article

Keywords:
MXene
Coating
Carbon nanocoil
Thermal diffusivity
Thermal conductivity

Timeline:
Received: October 27, 2021
Accepted: December 09, 2021
Published: December 27, 2021

Citation: Li Y, Wu F, Zhao S, Deng C. Thermal Diffusivity of $Ti_3C_2T_x$@C Nanocoils. J Adv Therm Sci Res. 2021; 8: 62-70.

DOI: https://doi.org/10.15377/2409-5826.2021.08.7

ABSTRACT

$Ti_3C_2T_x$ MXene is an emerging 2D material with excellent electrical and electrochemical properties. Carbon Nanocoil (CNC) is a quasi 1D material with unique helical morphology, which shows remarkable advantages in mechanical and electromagnetic properties. In this work, we designed a $Ti_3C_2T_x$@C nanocoil (CMNC) by coating $Ti_3C_2T_x$ flakes on the surface of CNC for better application performance. The thermophysical properties of single CMNCs were investigated using a transient electrothermal (TET) technique. The average room temperature thermal diffusivity and thermal conductivity of CMNCs were measured to be 8×10^{-6} m^2/s and 15.6 W/m K, respectively, which are one order of magnitude higher than those of CNCs, due to successful coating of MXene on the surface of CNC. However, the enhancement of electrical properties brought by MXene coating is much smaller than those of thermal properties. Variable temperature characterization from 298 to 334 K reveals an increasing trend of thermal diffusivity and thermal conductivity with increasing temperature, which is attributed to the interaction and heat transfer between MXene and CNCs. MXene coating provides better thermal management performance for practical applications of CNCs, such as wave absorbing.

*Corresponding Author
Email: cdeng@gxu.edu.cn
Tel: +86 19994407023

1. Introduction

Nanotechnology has come a long way in the past 30 years. Toward advanced electronics, energy conversion and storage, healthcare, catalysis and special industry, a variety of nanomaterials has been discovered and studied, including two outstanding representatives, carbon nanomaterials and transition metal carbonitride (MXene). Carbon nanocoil (CNC) is a carbon nanomaterial with unique spring-like morphology [1, 2]. Due to its helical morphology, CNC shows distinct advantages in mechanical and electromagnetic applications, such as wave absorbers and shields [3-5], composite materials [6], flexible sensors [7, 8], actuators [9], micro/nano electromechanical systems (M/NEMS) [10], nano-motor [11] and cold emitters [12]. Especially, the helical morphology of CNCs provides a good template for the growth of nanomaterials towards some certain applications, such as surface-enhanced Raman scattering (SERS) [13] and resonators of M/NEMS [14, 15].

MXene is an emerging two-dimensional material developed by the landmark work of Yury Gogotsi *et al*. [16] in 2011. Its molecular formula can be expressed as $M_{n+1}X_nT_x$, where M represents early transition metal atom, X is a carbon atom or nitrogen atom, and T_x corresponds to some surface groups, including OH, F and O. Due to wide selection of atoms, MXene represents a big family and shows wide applications, such as energy storage [17, 18], electromagnetic shields [19, 20], generator [21], catalysis [22, 23], flexible sensors [24-26] and transparent electrodes [27, 28], etc. The most studied MXene is $Ti_3C_2T_x$, which is also the first discovered MXene.

Utilizing the excellent electrical and chemical properties of MXene, quasi one-dimensional helical morphology and outstanding mechanical properties of CNCs, it is a good conception to combine $Ti_3C_2T_x$ and CNC together, which may integrate the advantages of them for better performance in a lot of applications, such as humidity sensors, infrared sensors, wave absorbers or shields, cold emitters and wearable sensors, *et al*. Towards practical applications, it is important to clarify the physics of this composite structure, including thermophysical properties, which determines the heat conversion, dispassion and detection of the composite. In this work, we coated $Ti_3C_2T_x$ flakes on the surface of CNC by simply mixing them together, forming a MXene@C nanocoil (CMNC). The thermophysics of single CMNCs were characterized using a simple but effective transient electrothermal (TET) technique. TET technique was developed by Guo *et al*. [29], which has been proven to be an accurate and reliable approach to measuring the thermal diffusivity of various solid materials, including conductive, semiconductive, or nonconductive materials [29-32]. The obtained results have high accuracy with less than 5% difference compared to the values in references. The detailed experimental process and principles for TET can be found in ref. [29]. Thermal diffusivity, thermal conductivity and electrical conductivity of CMNCs and their temperature dependence were characterized using variable temperature TET tests in the temperature range of 298 to 334 K. The role of MXene coating on the thermal physical properties of CMNC was analyzed.

2. Experimental

2.1. Synthesis of CNCs Using Chemical Vapor Deposition (CVD)

CNCs were synthesized using a chemical vapor deposition (CVD) method as reported [33]. Specifically, Fe^{3+} salt and Sn^{4+} salt with a molar ratio of 10:1 were dissolved in N, N-dimethylformamide (DMF). After 30 min ultrasonication, the mixture was transferred into a Teflon-lined stainless autoclave and heated at 180 °C for 30 h, followed by a natural cooling process. The generated catalyst powder was collected using vacuum filtration and washed with deionized (DI) water and absolute ethanol for three times, and finally dried at 60 °C for 3 h. For the CVD growth of CNCs, 20 mg catalyst powder was dispersed into 20 mL absolute ethanol. After ultrasonication for 30 min, 50 μL catalyst dispersions were spin-coated onto a Si substrate (15×15 mm^2). CNCs were synthesized on the substrate at 710 °C for 30 min by introducing a mixture of 235 sccm Ar and 25 sccm C_2H_2.

2.2. Synthesis of $Ti_3C_2T_x$ MXene

The delaminated $Ti_3C_2T_x$ MXene was synthesized according to a reported mild etching and delamination method with HCl/LiF [34]. Specifically, 1 g of LiF was dissolved in 20 mL of 9 mol/L HCl in a Teflon container under magnetic stirring for 10 min to ensure the dissolution of LiF. Thereafter, 1 g of Ti_3AlC_2 (MAX phase) powder was

slowly added to the LiF/HCl solution, and the mixture was moderately stirred at 50 °C for 24 h to allow sufficient etching of Ti_3AlC_2 and obtain a stable suspension. The obtained suspension was washed repeatedly with deionized water and centrifuged at 4000 rpm for 5 min until the pH of the supernatant was approximately 6.0. The obtained $Ti_3C_2T_x$ powder was dried under vacuum at 60 °C overnight. The delamination of $Ti_3C_2T_x$ powder was achieved by sonication for 30 min and mechanical shaking for 30 min, followed by centrifugation at 4000 rpm for 20 min.

2.3. TET Characterization of CMNCs and CNCs

TET characterization of CMNCs was conducted using a current source and an oscilloscope. A step current ranging from 5 to 10 μA was applied to single suspended CMNCs using the current source to generate Joule heating, and the oscilloscope was used to monitor the resistance evolution of the single CMNCs under Joule heating, which reflects the thermal diffusion process along the CMNCs. The tests were conducted in a vacuum chamber with an air presser smaller than 0.5 mTorr to reduce heat convection. Variable temperature TET characterization was carried out using a homemade heating stage. Detailed characterization principles and the preparation of suspended CMNCs will be discussed in the results chapter.

3. Results and Discussion

3.1. Structure of CMNCs

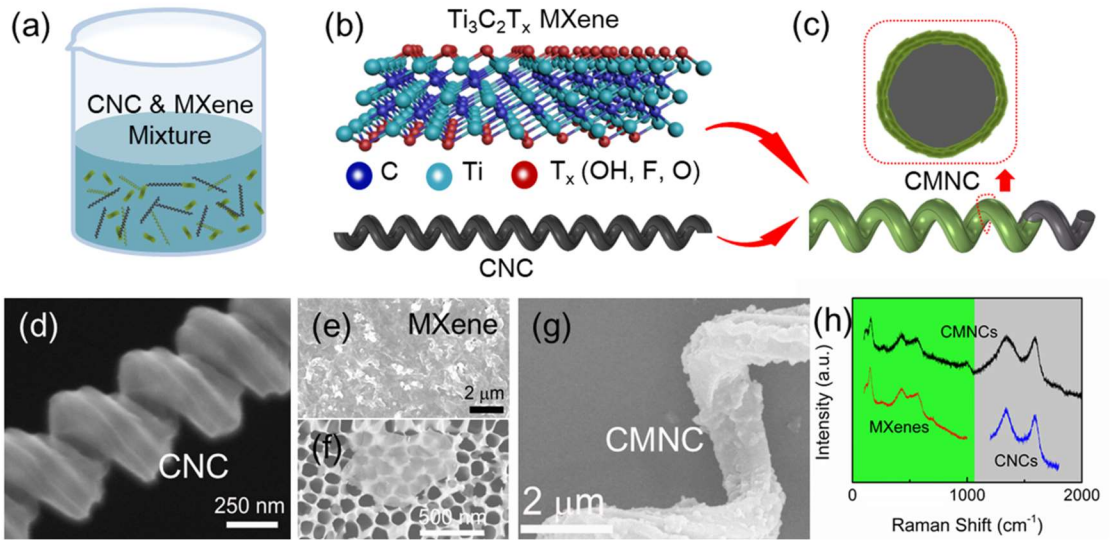

Figure 1: (a) Mixing CNC and MXene flakes with a mass ratio of 1: 2 for preparing CMNCs, (b) atomic structure of $Ti_3C_2T_x$ and helical morphology of CNC, (c) structural representation of CMNCs, where the green coating layer represents $Ti_3C_2T_x$ film, (d) SEM images of a single CNC, (e) $Ti_3C_2T_x$ films on a glass substrate, (f) a single $Ti_3C_2T_x$ flake on an anodised aluminium substrate, (g) a single CMNC, and (h) Raman spectrum of MXenes, CNCs and CMNCs.

For the preparation of CMNCs, the as-grown CNC clusters are scraped into the aqueous dispersion of $Ti_3C_2T_x$ flakes, with a mass ratio of 1:2. Benefiting from the helical morphology, CNCs are easy to disperse by using ultrasonic dispersion alone. $Ti_3C_2T_x$ flakes are adsorbed onto the surface of single CNCs through electrostatic interaction due to different charges on $Ti_3C_2T_x$ flakes and CNCs and Van der Waal forces between them, forming CMNCs. Figure **1a** shows a schematic for the mixture of CNCs and MXenes. Figures **1b** and c present the structure and morphology of $Ti_3C_2T_x$, CNC and CMNC. Figure **1d** shows the scanning electron microscope (SEM) image of a typical CNC, where a smooth surface of the CNC can be observed. Figures **1e** and f show the SEM images of $Ti_3C_2T_x$ films deposited on a glass substrate and a single $Ti_3C_2T_x$ flake on an anodised aluminium substrate. The average size of the as-prepared $Ti_3C_2T_x$ flakes is around 1 μm. Small size and atomic thickness make it possible for the conformal coating of $Ti_3C_2T_x$ flakes on the surface of a single CNC. Figure **1g** shows the SEM image of a typical CMNC. $Ti_3C_2T_x$ flakes are tightly wrapped around the CNC layer by layer, achieving a uniform and dense coating of $Ti_3C_2T_x$ flakes, which changes the surface of CNC into a rough one. Raman spectrum was employed to further

demonstrate the successful coating of $Ti_3C_2T_x$ flakes and characterize the structure of CMNCs. First, the Raman spectrums of MXenes and CNCs were acquired. Two characteristic peaks of CNCs (G and D peaks) and four characteristic peaks of $Ti_3C_2T_x$ can be identified [29, 35, 36]. The peaks of $Ti_3C_2T_x$ MXenes and CNCs locate in two different regions, 100-700 cm^{-1} and 1200-1800 cm^{-1} respectively, which make it facile to recognize the two components in a composite structure. The Raman spectrum of a single CMNC consists of all the characteristic peaks of $Ti_3C_2T_x$ flakes and CNC, which suggests a successful coating of MXene on the surface of CNC. For the Raman characterization of single CNCs and CMNCs, sputtered gold film (50 nm) on a glass substrate was employed to enhance the scattering signal due to the low Raman signal level of single nanowires.

3.2. TET Characterization of Single CMNCs

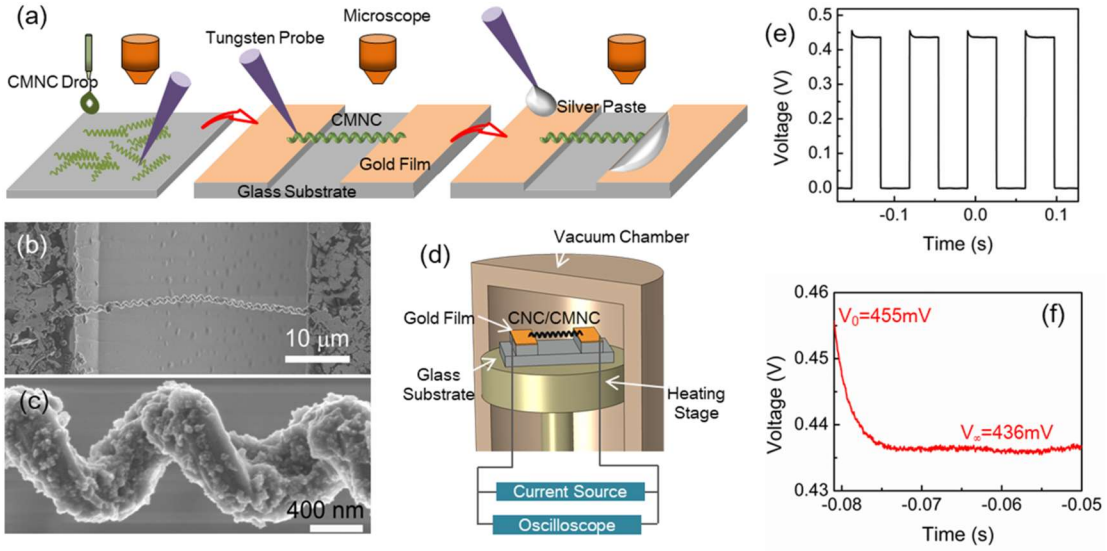

Figure 2: (a) Schematic illustration for the fabrication of suspended single CMNC device using micromanipulation technique, (b) SEM image of a typical CMNC device, (c) Enlarged SEM image of the CMNC in (b), (d) Schematic of TET characterization and experimental facility, (e) Typical voltage evolution curves, and (f) an enlarged view in one heating process during TET characterization.

For TET characterization, a suspended device should be prepared, as schematically shown in Figure **2a**. A small drop of the mixture of CNCs and MXene flakes is dropped onto a glass substrate. Then a single CMNC is picked out with a tungsten microprobe using a micromanipulator under a microscope and then transferred to a substrate with two separated gold electrodes with a 30-80 μm gap between them. The depth of the trench is about 200 μm, which is the thickness of the substrate coated with gold film. Silver paste carried on a tungsten probe is used to fix the single CMNC between the two electrodes and enhance electrical contact. Then the device is heated at 60 °C for 20 min to cure the silver paste before TET characterization. Figures **2b** and c show a typical suspended CMNC device and an enlarged view of the CMNC respectively. The length of the CMNC suspended between the two electrodes is about 40 μm.

Figure **2d** presents the schematic for the TET characterization of single CMNCs. The total tests were conducted in a vacuum chamber with air pressure smaller than 0.5 mTorr to reduce heat convection to a negligible level. A step current ranging from 5-10 μA was fed onto the single CMNC in the form of a square wave using a current source. The period of the square wave was set to be in the range of 25 to 100 ms, varying with the sample. The duty ratio of the wave was 50%. Due to Joule heating, the resistance of the single CMNC will decrease, resulting in a voltage decrease when the current is constant. An oscilloscope was used to record the voltage revolution with time. For a one-dimensional material, its heat transfer along the length direction is governed by,

$$\frac{\partial(\rho c_p T)}{\partial t} = \kappa \frac{\partial^2 T(x)}{\partial x^2} + \frac{I^2 R}{AL} - \frac{4\varepsilon\sigma_B(T^4 - T_0^4)}{d} \quad (1)$$

where *R*, *A*, *L*, *d*, κ and ρc_p are electrical resistance, cross-sectional area, length, diameter, thermal conductivity and specific heat of the 1D material, respectively. *I* is the applied current. $\sigma_B = 5.67\times10^{-8}$ W/ m^2 K^4 is the Stefan-Boltzmann constant. T_0 is ambient temperature, which is taken as the temperature of the electrodes as they can be seen as a heat sink for the heat dispassion of CNCs. Then the average normalized temperature rise due to Joule heating is given as

$$T^* = \frac{48}{\pi^4}\sum_{m=1}^{\infty}\frac{1-(-1)^m}{m^2}\frac{1-\exp(-m^2\pi^2\alpha_{measure}t/L^2)}{m^2} \tag{2}$$

where α_{measure} represents measured thermal diffusivity, which is a combination of real thermal diffusivity and radiation effect, and *t* is evolution time. Considering the helical morphology, the length *L* of a CMNC or a CNC sample is calculated as $\frac{L_0}{h}\sqrt{(\pi D)^2+h^2}$, where L_0 is the length of the nanowire measured directly through SEM image. *D* and *h* are the coil diameter and the pitch of the helical sample respectively. Temperature evolution determines the change of voltage. The normalized temperature rise can be expressed as $T^* = (V_{sample}-V_0)/(V_\infty - V_0)$, where V_0 and V_∞ are the initial and steady voltage in one heating process during TET characterization. The α_{measure} combining real thermal diffusivity and thermal radiation is expressed as

$$\alpha_{measure} = \alpha + \frac{1}{\rho c_p}\frac{8\varepsilon_r\sigma\overline{T}^3}{d}\frac{L^2}{\pi^2} \tag{3}$$

where α and ε_r are the real thermal diffusivity and effective heat emissivity of the sample respectively. Our previous works have demonstrated that the effect of thermal radiation on the total thermal diffusivity for such a 1D nanosystem is smaller than 5%, which can be neglected for our further analysis.

Figures **2e** and f present the voltage revolution curves of a typical sample in four heating-cooling processes and an enlarged view in one cycle. The gradual decrease of voltage with time represents the thermal relaxation along the length of this sample. Using a Matlab program for solving equation (2) to analyze this process, thermal diffusivity (α_{measure}) can be obtained. As a result, the average thermal diffusivity of three CMNC samples at room temperature (RT) is 8×10^{-6} m^2/s, which is much larger than that of pure CNCs as revealed in our previous work.

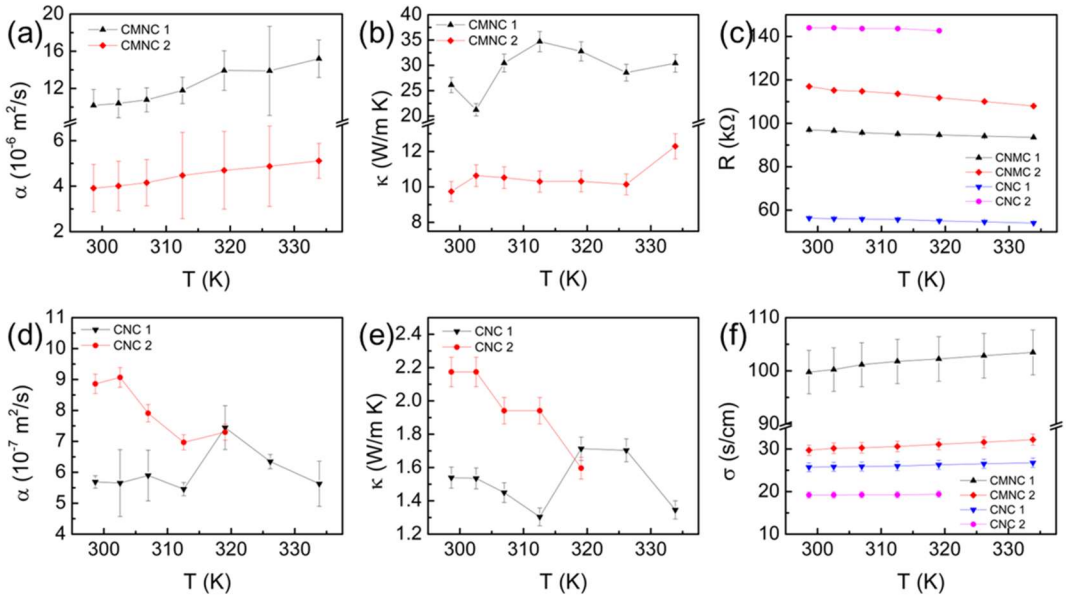

Figure 3: Variation of (a) thermal diffusivity (α), (b) thermal conductivity (κ) with temperature of two CMNC samples, (c) variation of resistance, (d) variation of thermal diffusivity (α), (e) thermal conductivity (κ) with the temperature of two CNC samples, and (f) electrical conductivity of the four samples.

For more in-depth research, variable temperature TET characterization (298-334 K) was carried out by heating the sample using a heating stage in the vacuum chamber. Figure **3a** shows the variation of thermal diffusivity for two CMNC samples, which increases from 10.1 to 15.2×10^{-6} m^2/s, and from 3.9 to 5.1×10^{-6} m^2/s for the two samples respectively, as temperature increases from 298 to 334 K. For a single material, thermal diffusivity always decreases with temperature increasing, due to enhanced phonon-phonon scattering. The increased thermal diffusivity of CMNCs uncovered here may be originated from the interaction between MXene flakes and CNC in this composite structure, which will be discussed later.

3.3. Thermal Conductivity of CMNCs

TET characterization is designed for probing the transient thermal diffusion process. For the characterization of thermal conductivity, steady thermal distribution should be built. Based on this concept, a steady electrothermal (SET) technique was employed. Along with the thermal relaxation, the temperature on single CMNCs will become stable. The temperature distribution derived from the governing equation of thermal balance can be expressed as

$$T(x) = -\frac{I^2 R_\infty}{AL}\frac{(x^2 - Lx)}{2\kappa} + T_0 \tag{4}$$

where $T(x)$ is the temperature at position x. R_∞ is the resistance of the sample at a steady state. T_0 is the temperature of the electrodes corresponding to ambient temperature. The average temperature along the CNC sample is calculated as

$$\overline{T(x)} = \int_0^L T(x)dx / L = \frac{I^2 R_\infty L}{12\kappa A} + T_0 \tag{5}$$

Thus, the average temperature rise is $\Delta T = I^2 R_\infty L / 12\kappa A$. The key point for calculating κ is obtaining the value of ΔT. As the resistance of CMNCs shows a correlation with temperature, the temperature rise on a CMNC can be reflected by the resistance change due to Joule heating. Resistance variations of the two CMNC samples are presented in Figure **3c**. In this small temperature range, the resistance can be linearly fitted. From the fitting curve, a differential of resistance *versus* temperature (dR/dT) can be obtained. Then the average temperature rise on the sample can be calculated using $\Delta T = \Delta R / (\mathrm{dR/dT})$, where ΔR corresponds to the difference of the resistance at the beginning (R_0) and the steady-state (R_∞) in one heating process. As results, the RT thermal diffusivities of the two CMNC samples are calculated to be 26.1 and 9.7 W/m K respectively. This value is consistent with the in-plane thermal conductivity of a composite film of MXenes and montmorillonite as reported, but much larger than that of CNCs in our previous work [32, 37]. Figure **3b** shows the variation of thermal conductivity for the two CMNC samples in the temperature range of 298 to 344 K, which shows about a 20% increase with temperature increasing, originating from the increase of thermal diffusivity.

For emphasizing the effect of MXene coating on the thermal transport of CMNCs, we carried out the TET characterization on two pure CNC samples. The average RT thermal diffusivity of the two CNCs is measured to be about 7.3×10^{-7} m^2/s, which is one order of magnitude smaller than that of CMNCs. Variable temperature characterization reveals a slight decrease of thermal diffusivity with temperature increasing, which obeys the prediction of phonon scattering theory. Using the temperature dependence curve of electrical resistance in Figure **3c**, the RT thermal conductivities of the two CNC samples are calculated to be 1.8 W/m K, which is in accord with the reported value [32]. With the temperature increasing, the thermal conductivity also shows a slightly decreasing trend. Due to the coating of $Ti_3C_2T_x$ flakes, the thermal conductivity and thermal diffusivity are both increased by one order of magnitude. However, the effect of $Ti_3C_2T_x$ coating on the electrical properties of the composite is much smaller than that on thermal properties. Figure **3f** shows the electrical conductivities of the four samples. Sample CMNC1 has the highest electrical conductivity, while that of sample CMNC 2 is comparable to that of samples CNC1 and 2. The average RT electrical conductivities of CMNCs and CNCs are 64.7 and 22.5 S/cm. Except for thermal diffusivity and conductivity, another important parameter of thermophysics is specific heat (c_p), which can be calculated as ($\kappa/\alpha\rho$). ρ is the mass density of the composite and simply taken as the density of CNC (graphite, 2200 kg/m^3). Then the average RT specific heat of CMNCs and CNCs are calculated to be 1148 and 1172 J/kg K respectively.

In the above calculation, we treated CMNC as a homogeneous material for simplicity. However, the thermal diffusion speed and temperature distribution in MXene coating layer and CNC are different, due to their different thermal diffusivity and conductivity. Then, there may be heat transfer between MXene flakes and CNC, resulting in a more complicated thermal governing equation. On the other hand, the interfacial charge transfer and interaction between MXene flakes and CNC may employ other influence factors for controlling the thermal and electrical transport in this composite structure. These two processes may result in increased thermal diffusivity with temperature increasing. To clarify the interaction between them and develop a more concise model to describe the thermal diffusion in CMNCs, more work needs to be done, which will be a focus of our future research.

4. Conclusion

In this work, we designed a MXene@C nanocoil (CMNC) by coating $Ti_3C_2T_x$ flakes on the surface of CNC. This coating process started from mixing CNCs and $Ti_3C_2T_x$ together and was accomplished by the electrostatic interaction between them. The thermal diffusion process of single CMNCs was characterized using TET technique, while the thermal conductivity was probed using SET technique. The average RT thermal diffusivity and thermal conductivity of CMNCs were measured to be 8×10^{-6} m^2/s and 15.6 W/m K, respectively, which are one order of magnitude higher than those of CNCs, due to successful coating of MXene on the surface of CNC. Variable temperature characterization uncovered the increased thermal diffusivity and thermal conductivity with temperature increasing, in the range of 298 to 334 K. This phenomenon is considered to be originated from the interfacial interaction and heat transfer between $Ti_3C_2T_x$ and CNC. Enhanced thermal diffusivity and conductivity provide better thermal management for the practical application of CNCs.

Acknowledgement

This work was supported by the National Natural Science Foundation of China (No.11904058), Guangxi Natural Science Foundation (2021GXNSFBA075039), Scientific Research and Technology Development Program of Guangxi (No. AD19245118).

References

[1] Ihara S, Itoh S, Kitakami J. Helically coiled cage dorms of graphitic carbon. Phys Rev B 1993; 48: 5643-5647. https://doi.org/10.1103/PhysRevB.48.5643

[2] Amelinckx S, Zhang X, Bernaerts D, Zhang X, Ivanov V, Nagy J. A formation mechanism for catalytically grown helix-shaped graphite nanotubes. Science 1994. https://doi.org/10.1126/science.265.5172.635

[3] Zhao Y, Zuo X, Guo Y, Huang H, Zhang H, Wang T, *et al*. Structural Engineering of Hierarchical Aerogels Comprised of Multi-dimensional Gradient Carbon Nanoarchitectures for Highly Efficient Microwave Absorption. Nano-Micro Lett 2021;13(9): 20. https://doi.org/10.1007/s40820-021-00667-7

[4] Zhao Y, Zhang H, Yang X, Huang H, Zhao G, Cong T, *et al*. In situ construction of hierarchical core-shell Fe3O4@C nanoparticles-helical carbon nanocoil hybrid composites for highly efficient electromagnetic wave absorption. Carbon 2021; 171: 395-408. https://doi.org/10.1016/j.carbon.2020.09.036

[5] Kang G H, Kim S H, Park S. Enhancement of shielding effectiveness for electromagnetic wave radiation using carbon nanocoil-carbon microcoil hybrid materials. Appl Surf Sci 2019; 477(5): 264-270. https://doi.org/10.1016/j.apsusc.2017.10.007

[6] Sanada K, Takada Y, Yamamoto S, Shindo Y. Analytical and Experimental Characterization of Stiffness and Damping in Carbon Nanocoil Reinforced Polymer Composites. J Solid Mecha Mater Engn 2008; 2(12): 1517-1527. https://doi.org/10.1299/jmmp.2.1517

[7] Yang S, Li C, Cong T, Zhao Y, Pan L. Sensitivity-Tunable Strain Sensors Based on Carbon Nanotube@Carbon Nanocoil Hybrid Networks. ACS Appl Mater Interf 2019; 11(41): 38160-38168. https://doi.org/10.1021/acsami.9b12600

[8] Wu J, Sun Y, Wu Z, Li X, Wang N, Tao K, Wang G. Carbon Nanocoil-Based Fast-Response and Flexible Humidity Sensor for Multifunctional Applications. ACS Appl Mater Interf 2019; 11(4):4242-4251. https://doi.org/10.1021/acsami.8b18599

[9] Ma H, Zhang X, Cui R, Liu F, Liu K. Photo-driven nanoactuators based on carbon nanocoil and vanadium dioxide bimorph. Nanoscale 2018; 10(23): 11158-11164. https://doi.org/10.1039/C8NR03622E

[10] Volodin A, Buntinx D, Ahlskog M, Fonseca A, Haesendonck C. Coiled Carbon Nanotubes as Self-Sensing Mechanical Resonators. Nano Lett 2004; 4(9): 1775-1779. https://doi.org/10.1021/nl0491576

[11] Li X, Sun Y, Zhang Z, Feng N, Song H, Liu Y, *et al*. Visible light-driven multi-motion modes CNC/TiO2 nanomotors for highly efficient degradation of emerging contaminants, Carbon 2019;155:195-203. https://doi.org/10.1016/j.carbon.2019.08.039

[12] Pan L, Hayashida T, Nakayama Y. Fabrication of Carbon Nanocoil Field Emitters and Their Application to Display. J Soci Photograph Sci Tech Jap 2002; 65(5):369-372.

[13] Li D, Pan L, Wu S, Li, S, An active surface enhanced Raman scattering substrate using carbon nanocoils. J Mater Res 2013; 28(16): 2113-2123. https://doi.org/10.1557/jmr.2013.212

[14] Deng C, Pan L, Li C, Fu X, Cui R, Nasir H. Helical gold nanotube film as stretchable micro/nanoscale strain sensor. J Mater Sci 2018; 53:2181-2192. https://doi.org/10.1007/s10853-017-1660-y

[15] Li C, Pan L, Deng C, Wang P. CNC-Al2O3-Ti: a new unit for micro scale strain sensing. Rsc Adv 2016; 6: 107683-107688. https://doi.org/10.1039/C6RA22361C

[16] Naguib M, Kurtoglu M, Presser V, Lu J, Niu J, Min H, *et al*. Two-dimensional nanocrystals produced by exfoliation of Ti3AlC2. Adv Mater 2011; 23(37): 4248-4253. https://doi.org/10.1002/adma.201102306

[17] Zhang C, Kremer K, Seral-Ascaso A, Park S, Mcevoy N, Anasori B, *et al*. Stamping of Flexible, Coplanar Micro-Supercapacitors Using MXene Inks. Adv Func Mater 2021; 31. https://doi.org/10.1002/adfm.202008795

[18] Yang X, Wang Q, Zhu K, Ye K, Yan J. 3D Porous Oxidation resistant MXene/Graphene Architectures Induced by In Situ Zinc Template toward High cc erformance Supercapacitors. Adv Funct Mater 2021; 31(20): 2101087. https://doi.org/10.1002/adfm.202101087

[19] Sun R, Zhang H, Liu J, Xie X, Yang R, Li Y, *et al*. Highly Conductive Transition Metal Carbide/Carbonitride(MXene)@polystyrene Nanocomposites Fabricated by Electrostatic Assembly for Highly Efficient Electromagnetic Interference Shielding. Adv Funct Mater 2017; 27(45):1702087. https://doi.org/10.1002/adfm.201702807

[20] Zhao S, Zhang H, Luo J, Wang Q, Xu B, Hong S, Yu Z. Highly Electrically Conductive Three-Dimensional Ti3C2Tx MXene/Reduced Graphene Oxide Hybrid Aerogels with Excellent Electromagnetic Interference Shielding Performances. Acs Nano 2018; 12(11):11193-11202. https://doi.org/10.1021/acsnano.8b05739

[21] Lee K, Zhang Y, Jiang Q, Kim H, Alkenawi A, Alshareef H. Ultrasound-Driven Two-Dimensional Ti3C2Tx MXene Hydrogel Generator. ACS Nano 2020;14(3):3199-3207. https://doi.org/10.1021/acsnano.9b08462

[22] L. Hu, M. Li, X. Wei, H. Wang, C. Zhu, Modulating Interfacial Electronic Structure of CoNi LDH Nanosheets with Ti3C2T MXene for Enhancing Water Oxidation Catalysis, Chem Engn J 2020;398:125605. https://doi.org/10.1016/j.cej.2020.125605

[23] Liu C, Li E. Termination Effects of Pt/v-Ti n+1CnT2 MXene Surfaces for Oxygen Reduction Reaction Catalysis. ACS Appl Mater Interfaces 2019; 11(1):1638-1644. https://doi.org/10.1021/acsami.8b17600

[24] Li S, Yu Z, Guo B, Guo K, Li Y, Gong L, *et al*. Environmentally stable, mechanically flexible, self-adhesive, and electrically conductive Ti3C2TX MXene hydrogels for wide-temperature strain sensing. Nano Energy 2021; 90:106502. https://doi.org/10.1016/j.nanoen.2021.106502

[25] Sharma S, Chhetry A, Zhang S, Yoon H, Park J. Hydrogen-Bond-Triggered Hybrid Nanofibrous Membrane-Based Wearable Pressure Sensor with Ultrahigh Sensitivity over a Broad Pressure Range. ACS Nano 2021; 15(3):4380-4393. https://doi.org/10.1021/acsnano.0c07847

[26] Wu M, He M, Hu Q, Wu Q, Zhou A. Ti3C2 MXene-Based Sensors with High Selectivity for NH3 Detection at Room Temperature. ACS Sens 2019; 4(10):2763-2770. https://doi.org/10.1021/acssensors.9b01308

[27] Park T, Yu S, Koo M, Kim H, Kim E, Park J, *et al*. Shape-Adaptable 2D Titanium Carbide (MXene) Heater. ACS Nano 2019;13(6):6835. https://doi.org/10.1021/acsnano.9b01602

[28] Chen J, Li Z, Ni F, Ouyang W, Fang X. Bio-inspired transparent MXene electrodes for flexible UV photodetector. Mater Horiz 2020; 7(7):1828-1833. https://doi.org/10.1039/D0MH00394H

[29] Guo J, Wang X, Wang T. Thermal characterization of microscale conductive and nonconductive wires using transient electrothermal technique. J Appl Phys 2007; 101: 063537. https://doi.org/10.1063/1.2714679

[30] Liu J, Qu W, Xie Y, Zhu B, Wang X. Thermal conductivity and annealing effect on structure of lignin-based microscale carbon fibers. Carbon 2017; 121:35-47. https://doi.org/10.1016/j.carbon.2017.05.066

[31] Xu Z, Wang X, Xie H. Promoted electron transport and sustained phonon transport by DNA down to 10 K. Polymer 2014;55(24): 6373-6380. https://doi.org/10.1016/j.polymer.2014.10.016

[32] Deng C, Sun Y, Pan L, Wang T, Xie Y, Liu J, *et al*. Thermal Diffusivity of Single Carbon Nanocoil: Uncovering the Correlation with Temperature and Domain Size. ACS Nano 2016; 10(10): 9710-9719. https://doi.org/10.1021/acsnano.6b05715

[33] Zhao Y, Wang J, Huang H, Cong T, Pan L. Growth of Carbon Nanocoils by Porous α-Fe2O3/SnO2 Catalyst and Its Buckypaper for High Efficient Adsorption. Nano-Micro Lett 2020; 12(1):23. https://doi.org/10.1007/s40820-019-0365-y

[34] Zhao X, Wang L, Tang C, Zha X, Yang W. Smart Ti3C2Tx MXene Fabric with Fast Humidity Response and Joule Heating for Healthcare and Medical Therapy Applications. ACS Nano 2020; 14(7): 8793-8805. https://doi.org/10.1021/acsnano.0c03391

[35] Sarycheva A, Gogotsi Y. Raman spectroscopy analysis of structure and surface chemistry of Ti3 C2Tx MXene. Chem Mater 2020; 32(8):3480-3488. https://doi.org/10.1021/acs.chemmater.0c00359

[36] Ferrari A. Interpretation of Raman Spectra of Disordered and Amorphous Carbon. Phys Rev. B, Cond Matt 2000; 61(20). https://doi.org/10.1103/PhysRevB.61.14095

[37] Deng C, Pan L, Ma H, Cui R. Electromechanical vibration of carbon nanocoils. Carbon 2015; 81: 758-766. https://doi.org/10.1016/j.carbon.2014.10.019

[38] Li L, Cao Y, Liu X, Wang J, Wang W. Multifunctional MXene-Based Fire-Proof Electromagnetic Shielding Films with Exceptional Anisotropic Heat Dissipation Capability and Joule Heating Performance. ACS Appl Mater Interfaces 2020; 12(24): 27350-27360. https://doi.org/10.1021/acsami.0c05692